AIAA Aviation
22-26 June 2015, Dallas, TX
33rd AIAA Applied Aerodynamics Conference

2015-2265

Slipstream Measurements of Small-Scale Propellers at Low Reynolds Numbers

Robert W. Deters*
Embry-Riddle Aeronautical University - Worldwide, Daytona Beach, FL 32114

Gavin K. Ananda† and Michael S. Selig‡
University of Illinois at Urbana-Champaign, Urbana, IL 61801

The continuing growth in the use of small UAVs has required the need to more fully understand the propellers that power them. Part of this understanding is the behavior of the propeller slipstream. Using a 7-hole probe, the slipstreams of several small-scale propellers (diameters of 4.2, 5, and 9 in) were measured in both static ($V_\infty = 0$) and advancing-flow ($V_\infty > 0$) conditions at several locations downstream. For static conditions, as the slipstream expanded downstream, the maximum values of the axial and swirl velocities decreased. The general shape of the static slipstream was also found to be nearly the same for the propellers even though their planforms were different. During advancing-flow conditions, a contraction in the slipstream occurred by 0.5 diameters behind the propeller. Beyond that location, the size of the slipstream was relatively constant up to 3 diameters downstream (furthest distance measured). For advancing-flow slipstreams, the shape of the axial velocity distribution was observed to be dependent on the planform shape of the propeller. The static slipstream of a propeller-wing configuration showed that the slipstream portions above and below the wing moved away from each other towards opposite wing tips. However, the maximum axial and swirl velocities in the propeller-wing slipstream did not diminish compared with the isolated propeller slipstream.

Nomenclature

A	=	propeller disk area
C_P	=	power coefficient
C_T	=	thrust coefficient
D	=	propeller diameters
J	=	advance ratio
n	=	propeller rotation rate (rot/sec)
p	=	pressure
q	=	dynamic pressure
R	=	propeller radius
r	=	distance along propeller radius
T	=	temperature
u, v, w	=	velocity components
V	=	velocity
V_∞	=	freestream velocity
V_T	=	tip speed
w	=	propeller induced velocity (theory)
x	=	distance downstream from propeller, distance along wingspan

*Assistant Professor, Department of Engineering Sciences, AIAA Member.
†Graduate Research Assistant, Department of Aerospace Engineering, AIAA Student Member.
‡Associate Professor, Department of Aerospace Engineering, AIAA Associate Fellow.

y = distance perpendicular to freestream, distance above or below wing

ρ = air density

I. Introduction

As the popularity of small Unmanned Air Vehicles (UAVs) has grown, the interest in the small propellers that power these vehicles has grown as well. Besides knowing the performance of these propellers in terms of thrust and power, it is also important to understand the effects of the slipstreams produced by these propellers. A propeller slipstream will not only affect any surfaces of the vehicle directly behind the propeller, but it also has the potential to affect other vehicles that are further away. It is foreseeable that these aircraft might fly in formations or swarms, so they will probably be flying in the wakes of one another. Since small UAVs are generally light in weight, they are more susceptible to any gusts.

To help understand the nature of the slipstream from small-scale propellers, a 7-hole probe was used to measure the flow behind these propellers. Several propellers were tested in both static ($V_\infty = 0$) and advancing-flow ($V_\infty < 0$) conditions, and slipstream profiles were measured at several locations downstream from the propeller. The effect of a wing on a propeller slipstream was also tested. A flat-plate wing was placed behind the propeller, and this wing-propeller slipstream was measured and compared to the slipstream of an isolated propeller.

II. Expected Slipstream Results from Theory

Before discussing the experimental procedure and the results from the slipstream measurements, a review of momentum theory for a propeller is useful in providing some background to what results are expected. Momentum theory is not derived in this paper as it can be found in many sources such as Johnson,[1] Leishman,[2] and McCormick.[3] The naming scheme for the variables in this section is similar to that used by McCormick.[3] The results from momentum theory will explain how a change in Reynolds number will affect the slipstream and how total pressure measurements can provide an estimate of the propeller thrust.

In momentum theory, the propeller is modeled as an actuator disk that has a discontinuous increase in static pressure. Figure 1 (adapted from McCormick[3]) shows how the flow around the propeller is modeled. Equations 1 and 2 show the results for the propeller thrust from using the momentum theorem.

$$T = \rho A_3 V_3 \left(V_3 - V_\infty\right) \tag{1}$$

$$T = A \left(p_2 - p_1\right) \tag{2}$$

An important result is that the velocity at the propeller disk can be found to be the average of the freestream velocity and the velocity far downstream.

$$V_1 = \frac{V_\infty + V_3}{2} \tag{3}$$

By introducing an induced velocity w, the velocity downstream can be defined as

$$V_3 = V_\infty + 2w \tag{4}$$

Using Eq. 4 with Eq. 3, the velocity at the propeller is now

$$V_1 = V_\infty + w \tag{5}$$

and the thrust can now be expressed as

$$T = 2\rho A w \left(V_\infty + w\right) \tag{6}$$

Solving for the induced velocity (Eq. 7) shows that disk loading (T/A) is an important factor. An increase in the disk loading will increase the induced velocity. This dependence on the disk loading can be used to explain how the Reynolds number will affect the slipstream of a propeller.

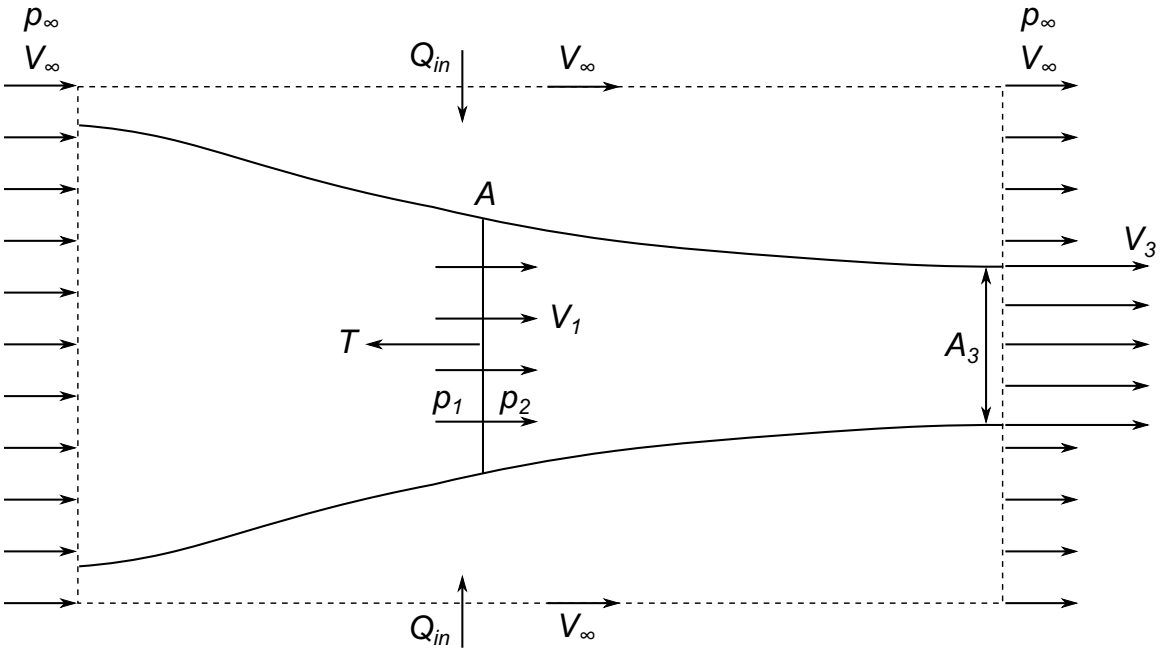

Figure 1: Flow around a propeller using momentum theory (adapted from McCormick[3]).

$$w = \frac{1}{2}\left[-V_\infty + \sqrt{V_\infty^2 + \frac{2T/A}{\rho}}\right] \tag{7}$$

During static conditions ($V_\infty = 0$), the induced velocity (Eq. 7) becomes

$$w = \sqrt{\frac{T/A}{2\rho}} \tag{8}$$

Deters et al.[4,5] showed that the Reynolds number can affect the thrust coefficient (C_T). A change in the thrust coefficient will directly affect the thrust by

$$T = \rho n^2 D^4 C_T \tag{9}$$

Substituting Eq. 9 and the equation for the disk area given by

$$A = \frac{\pi}{4} D^2 \tag{10}$$

into Eq. 8, the induced velocity can be written in terms of the thrust coefficient and the rotational rate. The resulting equation for the induced velocity is thus

$$w = \sqrt{\frac{2}{\pi} n^2 D^2 C_T} \tag{11}$$

The static induced velocity equation shows that an increase in the thrust coefficient or the rotational rate will increase the induced velocity. By dividing by the tip speed of the propeller ($V_T = \pi n D$), Eq. 11 becomes

$$\frac{w}{V_T} = \sqrt{\frac{2}{\pi^3} C_T} \tag{12}$$

Therefore, during static conditions, the ratio of the induced velocity to the tip speed is a function of the thrust coefficient.

The induced velocity in an advancing-flow slipstream is provided in Eq. 7. As shown in the equation, the freestream velocity has a direct effect on the magnitude of the induced velocity. By dividing the induced velocity by the freestream velocity, the ratio of the induced velocity to the freestream velocity is shown to be

$$\frac{w}{V_\infty} = \frac{1}{2}\left[-1 + \sqrt{1 + \frac{2T}{\rho A V_\infty^2}}\right] \tag{13}$$

Substituting in the thrust and disk area equations (Eqs. 9 and 10), as was done in the static case, results in

$$\frac{w}{V_\infty} = \frac{1}{2}\left[-1 + \sqrt{1 + \frac{8}{\pi}\frac{n^2 D^2 C_T}{V_\infty^2}}\right] \tag{14}$$

By using the definition of the advance ratio given by

$$J = \frac{V_\infty}{nD} \tag{15}$$

Eq. 14 becomes

$$\frac{w}{V_\infty} = \frac{1}{2}\left[-1 + \sqrt{1 + \frac{8}{\pi}\frac{C_T}{J^2}}\right] \tag{16}$$

Thus, for a propeller at a constant advance ratio, the ratio of the induced velocity to the freestream velocity is a function of the thrust coefficient.

A method to estimate the thrust of the propeller from pressure measurements is also a result from momentum theory. The rotational flow created by the propeller in the slipstream is ignored in classic momentum theory, so the total pressure upstream and downstream of the propeller can be written as

$$\text{Upstream: } p_{0_u} = p_\infty + \frac{1}{2}\rho V_\infty^2 = p_1 + \frac{1}{2}\rho V_1^2 \tag{17}$$

$$\text{Downstream: } p_{0_d} = p_\infty + \frac{1}{2}\rho V_3^2 = p_2 + \frac{1}{2}\rho V_1^2 \tag{18}$$

Subtracting Eq. 17 from Eq. 18 shows that the difference in the static pressure is the same as the difference in the total pressure.

$$p_{0_d} - p_{0_u} = p_2 - p_1 \tag{19}$$

So the relationship between the thrust and the pressure difference (Eq. 2) can be rewritten in terms of the total pressure.

$$T = A\left(p_{0_d} - p_{0_u}\right) \tag{20}$$

As stated earlier, the above equations assumed that the rotational flow behind the propeller can be ignored. Considering the rotational component, the total pressure upstream and downstream of the propeller is more correctly written as

$$\text{Upstream: } p_{0_u} = p_1 + \frac{1}{2}\rho V_1^2 \tag{21}$$

$$\text{Downstream: } p_{0_d} = p_2 + \frac{1}{2}\rho(v_x^2 + v_y^2 + v_z^2) \tag{22}$$

where v_x, v_y, and v_z are the components of the velocity in the slipstream in the axial, tangential, and radial directions, respectively. Equation 21 assumes that the total pressure ahead of the propeller is the same as the freestream total pressure. Stanton et al.[6] and Fage et al.[7] showed through experiments that the total pressure ahead of the propeller was measured to be the same as the freestream total pressure. If the tangential and radial components are small compared to the axial component, then Eq. 20 will provide a reasonable estimation of the thrust. Stanton et al.[6] and Fage et al.[7–9] showed in experiments that using the difference in total pressure did provide a close approximation to the thrust measured directly from the propeller as long as the propeller was not operating near static conditions.

(a) (b)

Figure 2: Photographs of the Aeroprobe 7-hole probe used during testing: (a) front view and (b) side view.

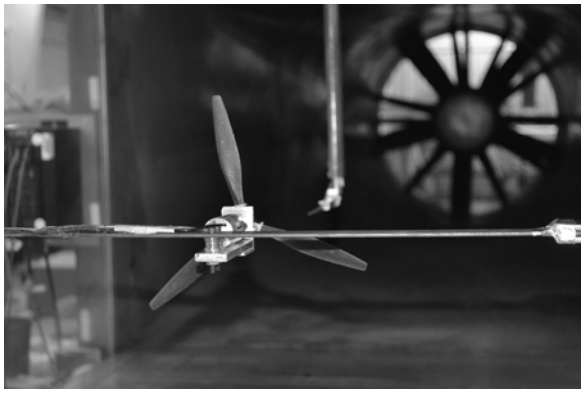

Figure 3: Experimental setup for propeller slipstream measurements (camera view pointing downstream).

III. Experimental Methodology

A. Experimental Setup

Slipstream measurements for an isolated propeller were conducted in the UIUC low-turbulence subsonic wind tunnel. The wind tunnel is an open-return type with a 7.5:1 contraction ratio. The rectangular test section is 2.8×4.0 ft (0.85×1.2 m) in cross section and is 8 ft (2.44 m) in length. To account for the boundary-layer growth at the side wall, the width of the test section increases by approximately 0.5 in (1.27 cm) over the length of the test section. In order to have low turbulence levels at the test section, a 4 in (10.2 cm) honeycomb and four anti-turbulence screens are in the settling chamber. The resulting turbulence intensity for an empty tunnel has been measured to be less than 0.1% at all operating conditions.[10] A 125 hp (93.2 kW) AC motor driving a five-bladed fan is used to control the test-section speed up to 235 ft/s (71.6 m/s). The maximum test-section speed for these tests was 40 ft/s (12.2 m/s). Test-section speeds were measured using a MKS 220 1-torr differential pressure transducer connected to static ports at the settling chamber and at the beginning of the test section. Ambient pressure was measured using a Setra Model 270 pressure transducer, and ambient temperature was measured using an Omega GTMQSS thermocouple.

Propeller slipstream measurements were taken using a 7-hole probe manufactured by Aeroprobe.[11] The advantage of using a 7-hole probe is that the static pressure, total pressure, and flow angles can be measured. From the pressures and flow angles, the three components of the flow velocity can be found. Pictures of the front and side views of the probe are shown in Fig. 2. The probe has a diameter of 0.125 in (3.2 mm), and the tip has a 30 deg conical shape with hole diameters of 0.020 in (0.51 mm). The experimental setup to measure the slipstream is shown in Fig. 3. The motor was mounted to a horizontal support beam that was upstream of the motor and propeller. The center of the propeller hub was aligned with the center of the support beam. While the support arm will affect the oncoming flow to the propeller, the slipstream was only measured in the vertical plane so the effect of the support arm was minimal.

Downstream of the propeller mount, the 7-hole probe was attached to two Zaber T-LST450B motorized linear slides. One slide moved the probe vertically while the other moved along the flow direction. A vertical slice of the propeller slipstream was taken at various points behind the propeller. The two Zaber slides were mounted outside of the test section on the ceiling. Each slide had a range of 17.7 in (45 cm), which allowed the slipstream to be measured three diameters downstream for 5 in propellers and 1.5 diameters downstream for 9 in propellers. To keep the test section closed, the slides were sealed in a box and were therefore at the same pressure as the tunnel. Each hole of the probe was attached to a MKS 220 1-torr pressure transducer where the tunnel static pressure was used as the reference. During static tests, the tunnel side walls were

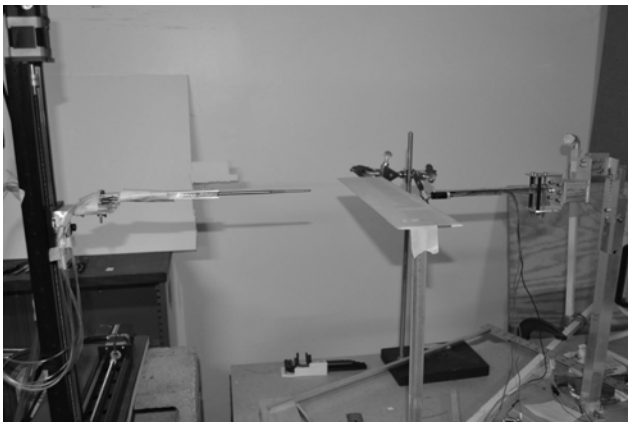

Figure 4: Experimental setup to measure the effect of a flat-plate wing on the slipstream of a propeller.

opened in order to keep the tunnel test section at atmospheric pressure. The MKS pressure transducer used for each hole was the same as the one used during calibration. Using the same pressure transducers ensured that any errors in the transducer calibration slopes were taken into account in the 7-hole probe calibration data.

A second setup was used to measure the effect of a flat-plate wing on the static slipstream of a propeller (Fig. 4). These tests were performed outside of the wind tunnel. The flat-plate wing used in this study had a chord of 3.5 in, a thickness of 4.3%, and an aspect ratio of 4. The airfoil for the wing had a 5-to-1 elliptical leading edge and a 10-to-1 elliptical trailing edge. The wing was rapid prototyped using SLA, and more information can be found in Ananda et al.[12,13]

The wing was placed behind the propeller at two different locations, and several propellers were tested. The 7-hole probe was attached to the two Zaber slides in order to gather several vertical slices of data along the span of the wing. One Zaber slide moved in the vertical direction while the other moved in the wingspan direction. Three locations behind the wing-propeller were measured, and for each location the 7-hole probe and Zaber setup was moved so that the front of the probe was at the desired location.

B. 7-Hole Probe

As mentioned earlier, the 7-hole probe was used because it provides total pressure, static pressure, and the flow angle at a point in the slipstream. With the pressures and flow angle, the three components of the flow velocity can be found. Since it is a pressure probe, the results found are the average conditions at that probe location. A detailed explanation of the theory behind a 7-hole probe is not provided here, but it can be found in Gallington et al.,[14,15] Zilliac,[16,17] and Deters.[4]

To use the 7-hole probe accurately, calibration was performed at the flow velocities expected. The purpose of calibration is to determine pressure calibration coefficients at known flow angles and at known total and static pressures. These calibration coefficients are then in turn used to determine the flow angle, total pressure, and static pressure in an unknown flow. While these coefficients should be generally velocity independent for incompressible flows, the Reynolds numbers expected for the slipstream measurements were low. The calibration flow speeds of 10, 20, 30, and 40 ft/s (3.0, 6.1, 9.1, and 12 m/s) had Reynolds numbers, based on the hole diameter, of approximately 100, 200, 300, and 400, respectively. According to Barker[18] and Bryer et al.,[19] the measurement of dynamic pressure as

$$q = \frac{1}{2}\rho V^2 \tag{23}$$

starts to not hold true when the Reynolds number of a total pressure probe hole is around 100. By calibrating at these four speeds, any Reynolds number effects will be taken into account.

A total of 2052 calibration points were taken at each flow speed, and flow angles went up to 56 deg. While a 7-hole probe is capable of measuring flow angles of 80 deg, the flow angles during calibration were kept at a maximum of 56 deg due to a physical constraint in the calibration setup. The wind tunnel turntable

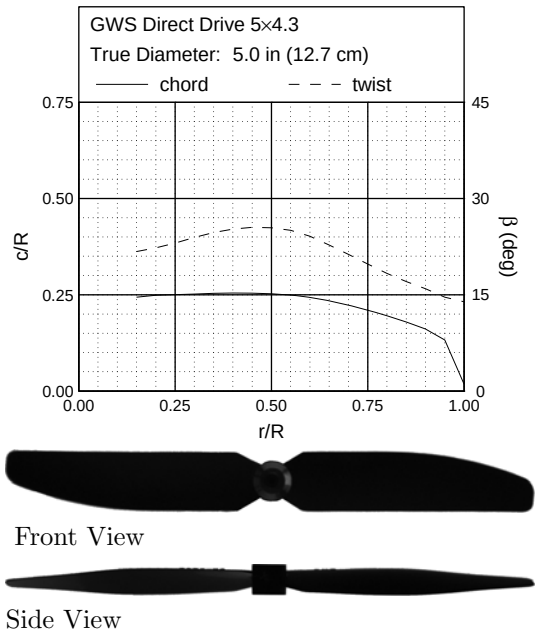

Figure 5: GWS Direct Drive 5×4.3 geometric characteristics.

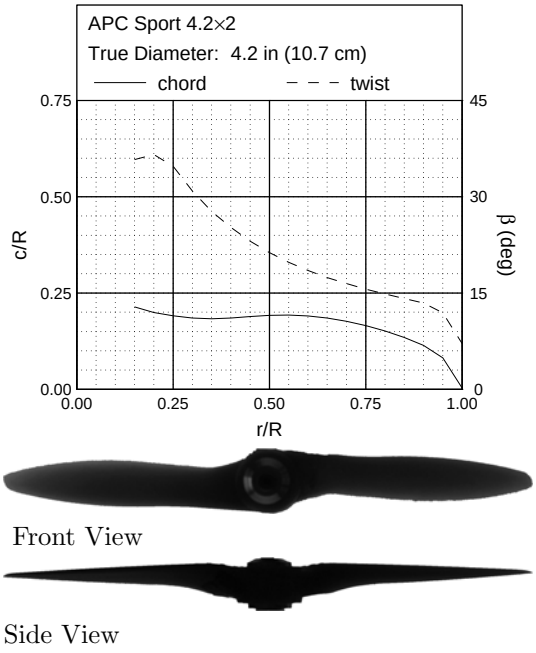

Figure 6: APC Sport 4.2×2 geometric characteristics.

limited the flow angle to 56 deg. At that angle and at the maximum calibration speed (40 ft/s), the pressure transducers were also near their operational limits.

To test the calibration data, a set of 99 points of known flow velocity and angle were measured using the 7-hole probe. From these test points, the average difference in velocity was found to be less than 0.2 ft/s, and the average difference in flow angle was less than 1.1 deg. The largest difference between known values and those found with the 7-hole probe were usually when the velocity was below 5 ft/s.[4]

When using the 7-hole probe to take flow measurements, an average of three 3-second measurements was used. Since there were four sets of calibration coefficients (one for each calibration flow speed), each measurement resulted in four solutions. To determine which set to use as the final result, the calculated velocity is used. While the four sets will provide slightly different results, there is usually only a few percent difference in the calculated velocities. If the calculated velocity is close to one of the calibration flow speeds (10, 20, 30, or 40 ft/s), then that flow speed calibration set is used. If the calculated velocity falls between two calibration flow speeds, then the results from the two calibration sets were interpolated.

C. Propellers

The slipstream results from several propellers are discussed in this paper. Two propellers (GWS Direct Drive 5×4.3 and APC Sport 4.2×2) were off-the-shelf and five propellers (5 in and 9 in DA4002, 5 in and 9 in NR640, and 9 in DA4022) were created using an Objet Eden 350 3D printer. A discussion on the design and manufacturing of the 3D-printed propellers can be found in Deters et al.[4,5] The geometry of the seven propellers are provided here and can also be found in Deters[4] and on the APA Propeller Database.[20] Figure 5 is for the GWS 5×4.3, and Fig. 6 is for the APC 4.2×2. The geometries for the two DA4002 propellers are shown in Figs. 7 and 8. The 5 in and 9 in NR640 propellers are provided in Figs. 9 and 10, respectively. Figure 11 shows the 9 in DA4022 propeller.

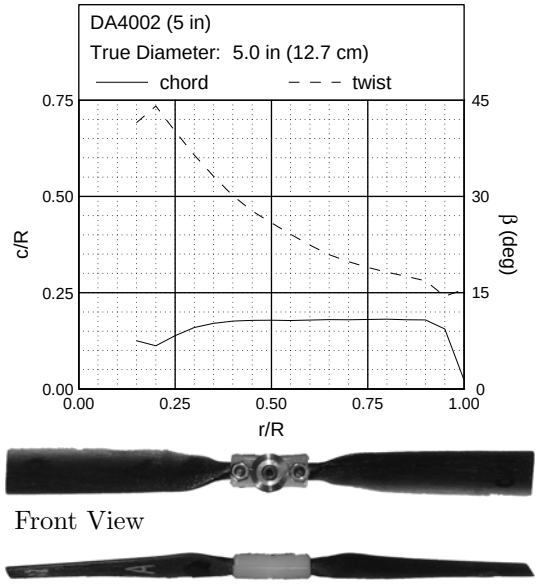

Figure 7: 5 in DA4002 geometric characteristics.

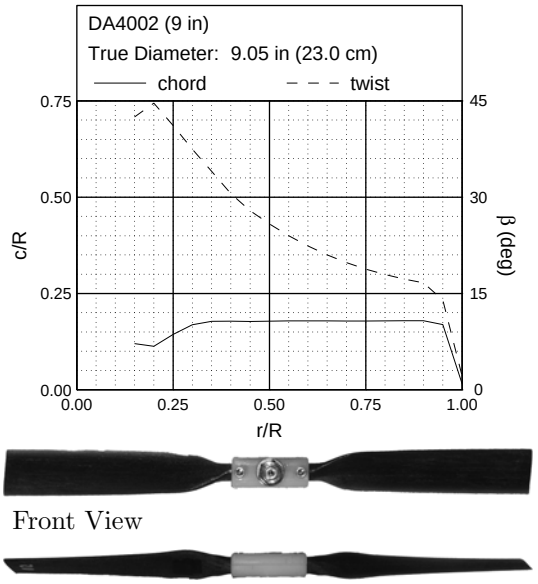

Figure 8: 9 in DA4002 geometric characteristics.

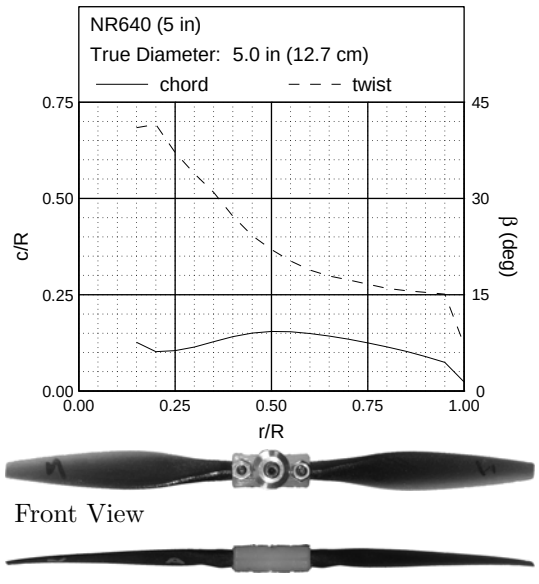

Figure 9: 5 in NR640 geometric characteristics.

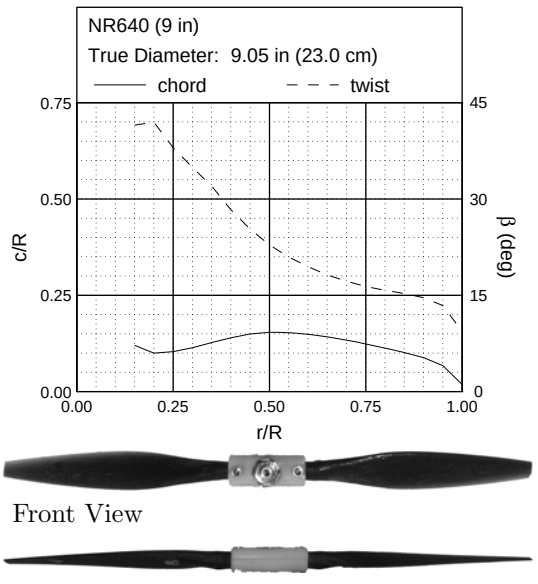

Figure 10: 9 in NR640 geometric characteristics.

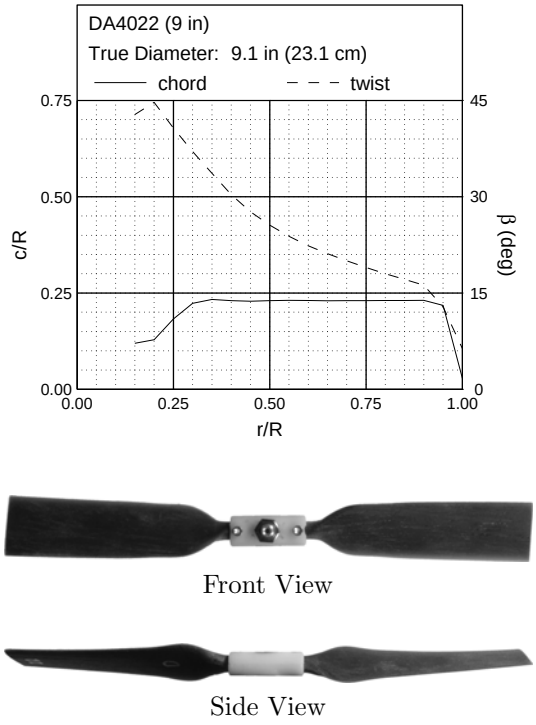

Figure 11: 9 in DA4022 geometric characteristics.

IV. Propeller Slipstream Measurements

As stated in Section III, vertical slices of the propeller slipstream were taken at different locations downstream from the propeller. Each vertical slice is representative of the shape of the full slipstream of an isolated propeller. Propeller slipstream measurements in both the static and advancing-flow conditions are presented in this section. The effect on the slipstream from a flat-plate wing placed behind a propeller was also measured during static conditions, and since the slipstream was no longer axisymmetric, multiple vertical slices of the slipstream were taken. More slipstream results can be found in Deters.[4]

A. Static Conditions

The slipstreams from a variety of propellers were taken during static conditions in order to determine their general characteristics. Results from two propellers (GWS 5×4.3 and APC 4.2×2.2) are presented here. Figure 12 shows the slipstream measurements in the axial direction of the GWS 5×4.3 propeller at 5,000 RPM at various locations behind the propeller. A picture of the propeller is provided on the left side of the figure for reference. The location of the propeller (center of the hub) during testing was at $x/D = 0$. Only the top half of the propeller slipstream was measured since it was assumed that the slipstream was symmetric. Each arrow in the figure shows the magnitude and direction of each slipstream measurement. For the slipstream profiles closer than $x/D = 0.5$, some blade locations do not show a velocity measurement. Since the 7-hole probe was limited to being able to measure flow angles up to 56 deg due to calibration limitations, an attempt was made to see if additional velocities could be measured at the closest location behind the propeller by changing the 7-hole probe orientation. This attempt did not provide any additional measurements near the propeller tip or near the hub. The 7-hole probe provides an average velocity measurement, so any velocities near the tip or hub could be too unsteady for a good measurement.

From the static performance results[4,5,20] (Fig. 13), the C_{T_0} and C_{P_0} are 0.15 and 0.080, respectively. The velocity measurements shown in Fig. 12 are a good representation of the general trends found in a static slipstream. As seen in the figure, beyond $x/D = 0.5$, the slipstream starts to expand as the maximum velocity in the slipstream starts to decrease and move towards the center of the slipstream. The expansion

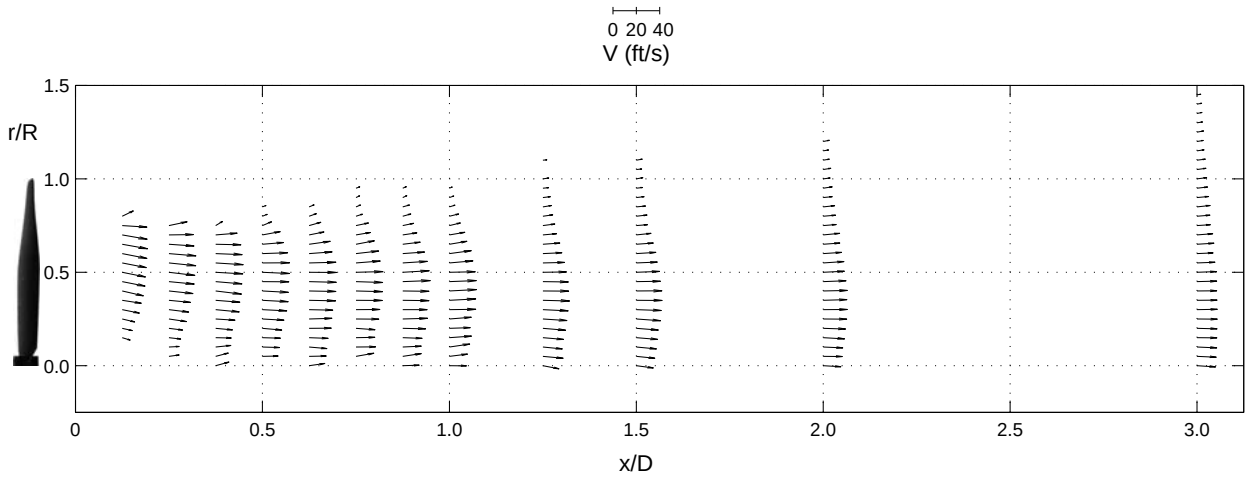

Figure 12: Slipstream of the GWS 5×4.3 propeller during static conditions at 5,000 RPM.

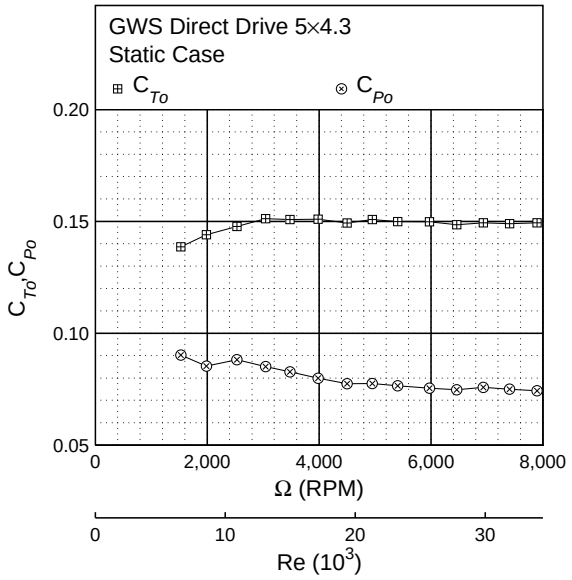

Figure 13: GWS Direct Drive 5×4.3 static performance.

of the slipstream looks fairly linear, and a linear fit through the outermost measured velocities gives an expansion angle of approximately 6.7 deg. Most of the expansion angles from other propellers tested fall between 6 and 8 deg.

Swirl measurements for the GWS 5×4.3 are shown in Fig. 14. Similar to the axial measurements, the maximum swirl value decreases as the slipstream expands, but it is still measurable three diameters downstream. Again a picture of the propeller is provided for reference. As shown, the propeller direction of rotation is counter-clockwise. The arrows in the figure show the measured velocity magnitude and direction.

To show the trends more clearly, Figs. 15a and 15b show the axial and swirl velocities, respectively, of the slipstream of the GWS 5×4.3 at 5,000 RPM. The axial velocity is represented by u, and the swirl velocity is represented by v. For these plots, the swirl velocity is taken to only be the tangential velocity. As seen in Fig. 15a, the slipstream spreads out, and the maximum velocity moves towards the propeller center. From Fig. 15b, the swirl stays about the same until $x/D = 1$ where it lessens and spreads out.

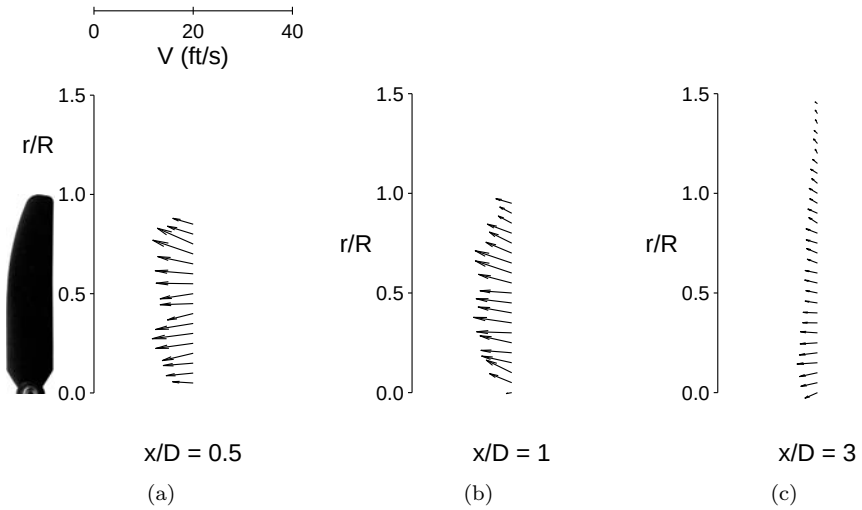

(a) (b) (c)

Figure 14: Swirl measurements of the GWS 5×4.3 at 5,000 RPM: (a) $x/D = 0.5$, (b) $x/D = 1$, and (c) $x/D = 3$.

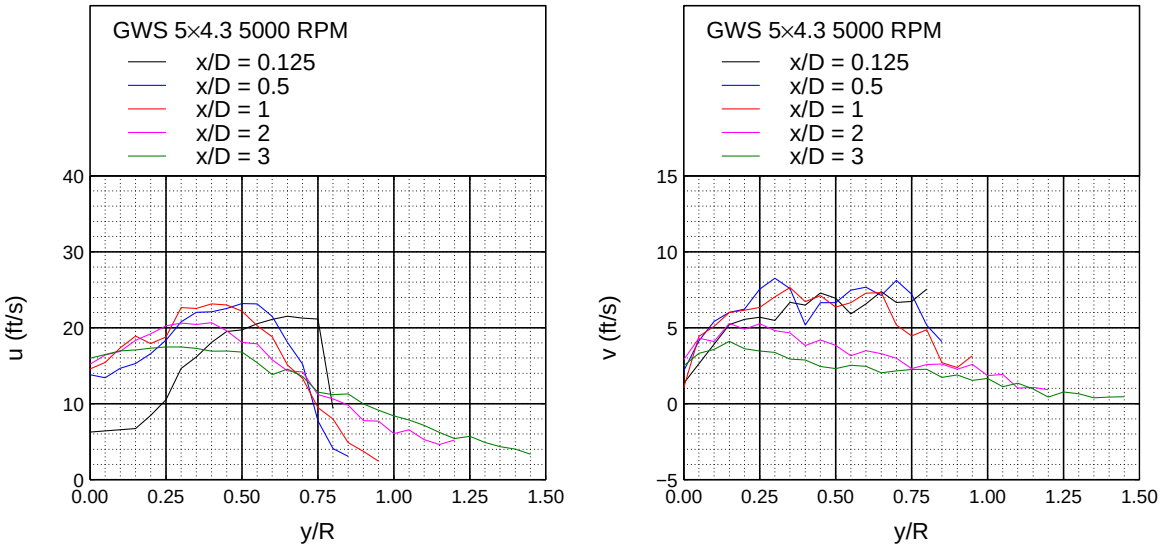

(a) (b)

Figure 15: Velocity measurements from the slipstream of the GWS 5×4.3 at 5,000 RPM: (a) axial velocity and (b) swirl velocity.

From the discussion on the induced velocity from momentum theory (Section II), it was shown that the ratio of the induced velocity to the tip speed is a function of the thrust coefficient. For many of the small-scaled propellers tested by Deters et al.,[4,5,20] an increase in the Reynolds number (propeller RPM) led to an increase in the thrust coefficient. Therefore, it is expected that the thrust coefficient increase will also increase the induced velocity ratio. While momentum theory ignores the effects of swirl, the increase in the induced velocity ratio from Eq. 12 should still be seen as an increase in the ratio of the axial velocity to the tip speed.

To demonstrate this Reynolds number effect on the propeller slipstream, measurements were taken of the APC 4.2×2 propeller at two rotational speeds: 9,000 RPM and 12,000 RPM. Figure 17 shows the axial and swirl velocities at 9,000 RPM. Similar to the GWS propeller, the maximum axial velocity past $x/D = 0.5$ lessens and moves towards the center, and the swirl lessens as it moves downstream. A comparison between

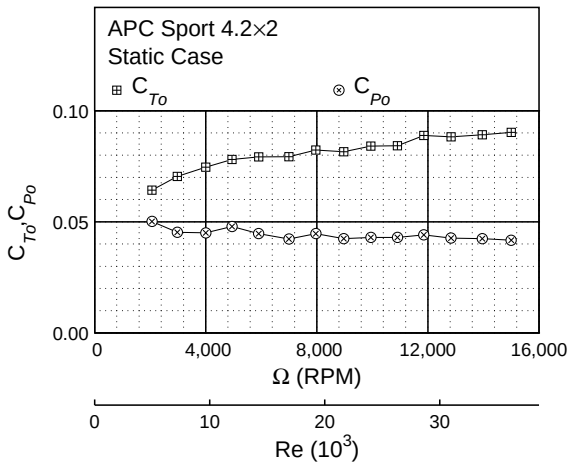

Figure 16: APC Sport 4.2×2 static performance.

the two rotational speeds for the APC propeller is shown in Fig. 18. The faster rotational rate leads to a higher thrust and therefore a larger axial flow as seen in the figure. The increase in the thrust also causes an increase in the induced power, so an increase in the swirl velocities is also seen. While the magnitudes of the velocities for the 12,000 RPM case are larger, the shape of the slipstream is the same between the two rotational rates.

Figure 19 shows the axial and swirl velocities divided by the tip speed. For the three downstream locations shown, the larger rotational speed produces a larger u/V_T and v/V_T. From the static performance results (Fig. 16),[4,5,20] the static thrust coefficient is 0.082 at 9,000 RPM and is 0.089 at 12,000 RPM. Using Eq. 12, momentum theory predicts that the increase in u/V_T would be 4.2%. Using the maximum axial velocity, the increase in u/V_T at $x/D = 0.5$ is 2.6%.

The results from the APC propeller show that the Reynolds number effect on the static thrust coefficient is also seen in the slipstream measurements. The increase in the axial velocity ratio predicted by momentum theory was greater than the amount measured from the slipstream, but the predicted increase is still useful. Using the results from Eq. 12, a static propeller slipstream at a known thrust coefficient can be scaled to another thrust coefficient. The amount of scaling given by momentum theory was shown to be greater than actual measurements, and the amount of scaling should be lessened.

While the two propellers discussed here had different planforms, the general shape of the velocity profiles are about the same. For the axial velocity at locations near the propeller, the maximum velocity is close to the 75% blade station. The peak velocity moves to around 50% around $x/D = 0.5$ and 1. At $x/D = 2$, the peak is around 25%, and by $x/D = 3$, the peak is nearly at the center of the propeller. For the swirl velocity, the pattern is more varied, but by three diameters downstream, the swirl has basically evened out. While results for only two propellers are shown, the same patterns in axial and swirl velocities are seen in the other propellers tested.[4] The results of these slipstream measurements follow the same trends as the propeller slipstream model developed by Khan and Nahon.[21]

B. Advancing-Flow Conditions

Slipstreams measurements were taken for a variety of propellers in an advancing flow. A typical advancing-flow slipstream is shown in Fig. 20 for the GWS 5×4.3 propeller at 5,000 RPM and 18 ft/s ($J = 0.52$). The vectors show the direction and magnitude of the measured velocity behind the propeller in the axial direction. As shown in the figure, a slipstream in an advancing flow is much different than the static slipstream (Fig. 12). Instead of expanding like the static slipstream, the shape of the advancing-flow slipstream seems to not vary. The swirl measurements for the propeller at the same conditions are shown in Fig. 21. The swirl velocities stay fairly consistent at the different points downstream.

Similar to the static slipstream discussion, Fig. 22 shows the axial and swirl velocities more clearly. As seen in the figure, the slipstream width decreases shortly behind the propeller (by $x/D = 0.5$) and the edge

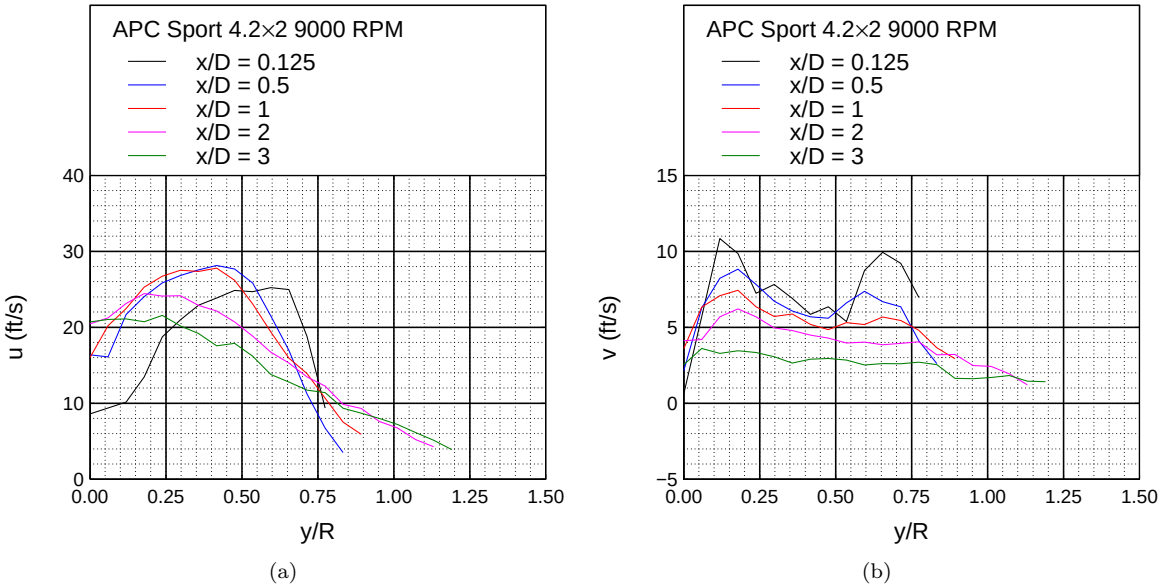

Figure 17: Velocity measurements from the slipstream of the APC 4.2×2 at 9,000 RPM: (a) axial velocity and (b) swirl velocity.

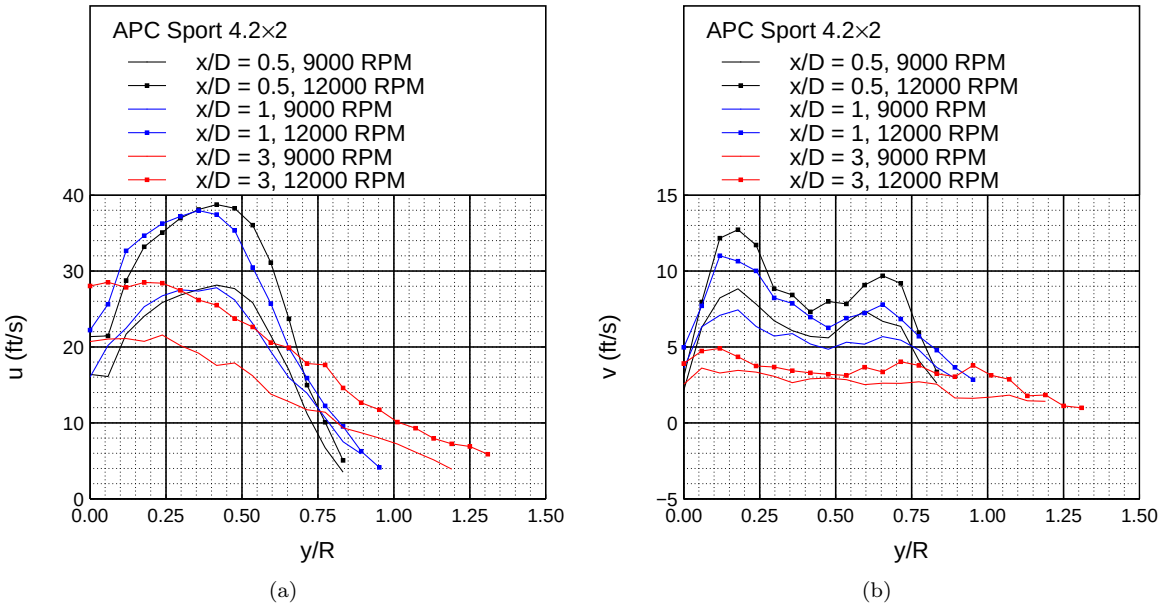

Figure 18: Velocity measurements from the slipstream of the APC 4.2×2 at 9,000 and 12,000 RPM: (a) axial velocity and (b) swirl velocity.

of the slipstream starts to smooth out as the slipstream travels further downstream. The axial velocity at the center of the propeller increases as the slipstream moves downstream. The initial deficit is due to the propeller hub and motor blocking the flow. The swirl profile does not change much at the different downstream locations.

The thrust and power coefficients for the GWS propeller in an advancing flow are shown in Fig. 23. As was seen in the static performance, there is little if any change in the thrust coefficient as the rotation speed (Reynolds number) increases. From the momentum theory discussion in Section II, the ratio of the induced

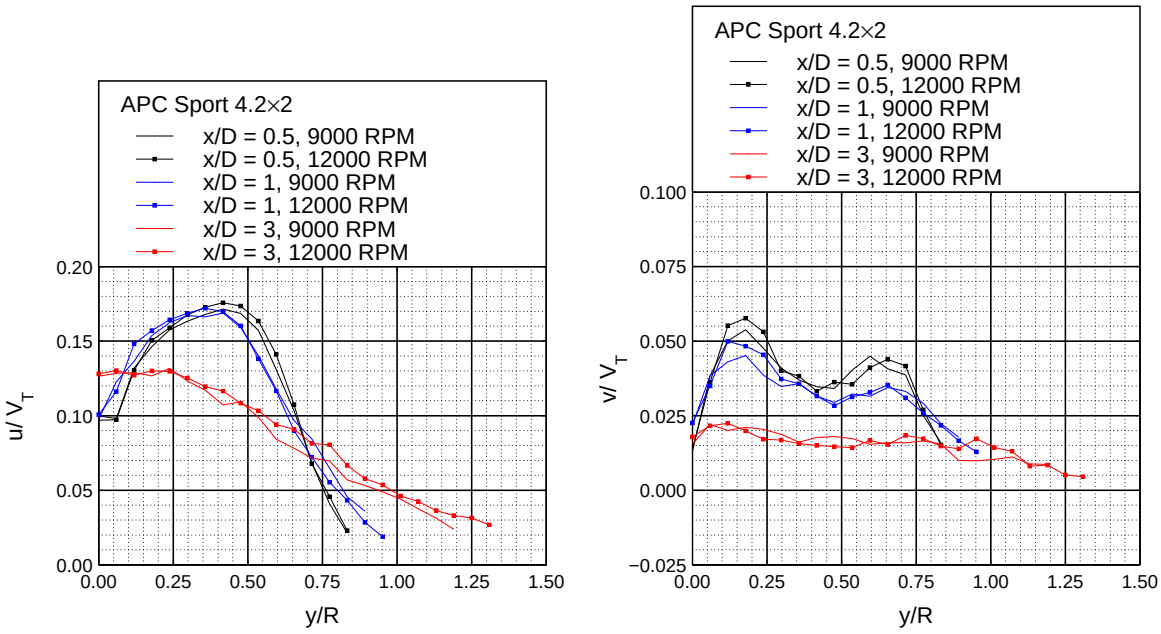

(a) (b)

Figure 19: Velocity measurements from the slipstream of the APC 4.2×2 at 9,000 and 12,000 RPM: (a) u/V_T and (b) v/V_T.

velocity to the freestream velocity for a propeller at a constant advance ratio is a function of the thrust coefficient (Eq. 16). Since there is no change in C_T at a constant advance ratio, then no change in the ratio of the induced velocity to the freestream velocity is expected.

While many of the propellers tested did show an increase in C_T with an increase in the rotational speed, it was difficult to show any significant change in the slipstream measurements. There were two main factors leading to this difficulty. The first was that many of the propellers only showed a small change in C_T, so only a small change in the induced flow ratio would be expected. The second was that the advance ratio is required to be constant in order to accurately show the effect of C_T. The advance ratio is part of Eq. 16, so any change will also affect the expected results. The 9 in DA4002 propeller was selected to show the effect of an increase in C_T due to the large measurable difference in C_T seen in its performance results (Fig. 24).[4,5,20] At an advance ratio of 0.64, the thrust coefficient at 2000 RPM was 0.047 and at 5000 RPM was 0.056.

The slipstream measurements of the 9 in DA4002 propeller at 5,000 RPM and 40 ft/s ($J = 0.64$) are shown in Fig. 25. Similar to the GWS 5×4.3, the slipstream contracts downstream, and the axial velocity increases downstream. Unlike the static slipstreams, the axial velocity profiles do not look the same between two different propellers. The GWS propeller has a more rounded profile where the peak is around the 60% blade station, but the DA4002 profile is more linear and the axial velocity continuously increases from the 30% station until its maximum around 80%. Having different axial velocity profiles between the two propellers is not surprising given that the two propellers have different chord and twist distributions. The swirl velocity profiles are similar between the two propellers.

As mentioned earlier, the 9 in DA4002 slipstreams were measured to see the effect of an increasing thrust coefficient. Figure 26 shows slipstream measurements taken at two different rotational rates (Reynolds numbers). As predicted by Eq. 16, the axial velocity ratio (u/V_∞) increased when the thrust coefficient increased at the same advance ratio (Fig. 26b). At each downstream location, the axial velocity ratio measured at 5,000 RPM was larger than at 2,000 RPM.

The 9 in DA4002 was also tested at a constant rotational speed with changes in the freestream velocity and thereby changing the advance ratio. Figure 27 shows the propeller at 5,000 RPM and at 34 and 40 ft/s. These conditions correspond to advance ratios of 0.57 and 0.64. As the advance ratio increases, the difference between the axial velocity behind the propeller and the freestream velocity decreases, and the magnitude of

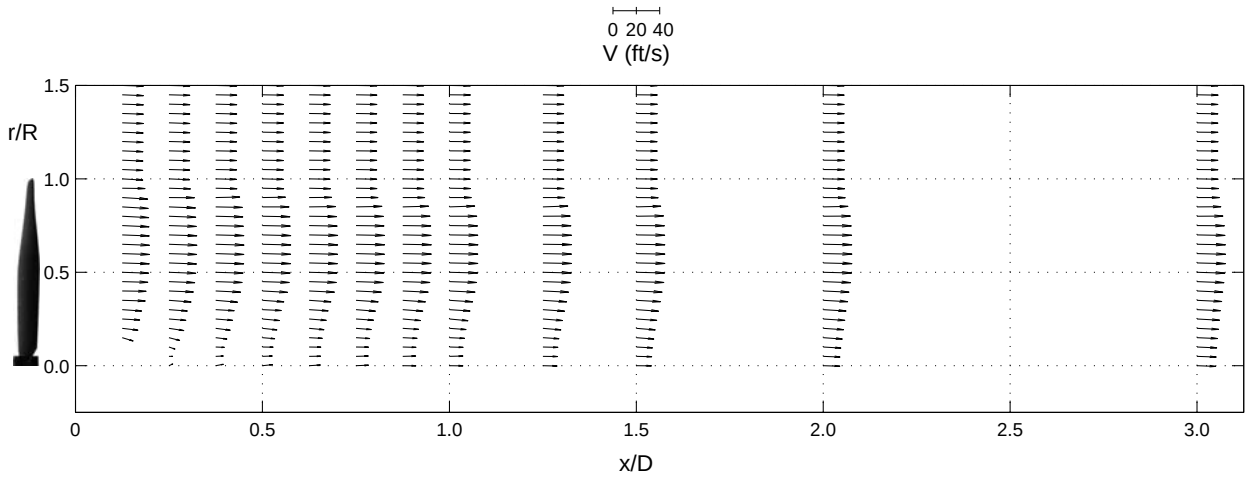

Figure 20: Slipstream of the GWS 5×4.3 propeller at 5,000 RPM and 18 ft/s ($J = 0.52$).

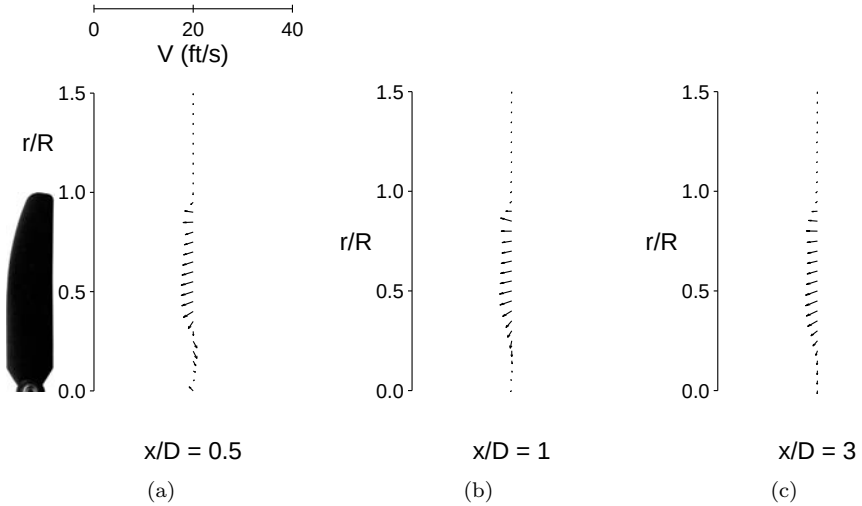

(a) (b) (c)

Figure 21: Swirl measurements of the GWS 5×4.3 at 5,000 RPM and 18 ft/s ($J = 0.52$): (a) $x/D = 0.5$, (b) $x/D = 1$, and (c) $x/D = 3$.

the swirl decreases. These decreases in the velocities directly show a decrease in the thrust and power of the propeller as the advance ratio increases.

Unlike the static slipstreams, the advancing-flow slipstreams do not expand downstream after the initial contraction. The GWS propeller showed that by three diameters downstream, the edge of the advancing-flow slipstream does become less defined, and there is less of a sudden change between the velocities in and out of the slipstream. At three diameters downstream, however, the swirl is still present, and the magnitude has not diminished. The behavior of the swirl agrees with slipstream measurements taken by Pannel and Jones who were able to measure swirl 8 diameters behind a propeller.[22] Another difference between the static and advancing flow slipstreams is the profile shape of the axial velocity. For the static slipstreams, the axial velocity profiles generally had the same shape and only the magnitude differed. For the advancing-flow slipstreams, the axial velocity profiles are dependent on the propeller geometry. However, the swirl velocity profiles for an advancing flow were very similar in shape for each propeller.

As discussed in Section II, the total pressure measurements of the slipstream can be used to estimate the thrust produced by the propeller. As was suggested in the literature,[6–9] the total pressure measurements from the closest downstream location ($x/D = 0.125$) were used. Static slipstreams underestimated the

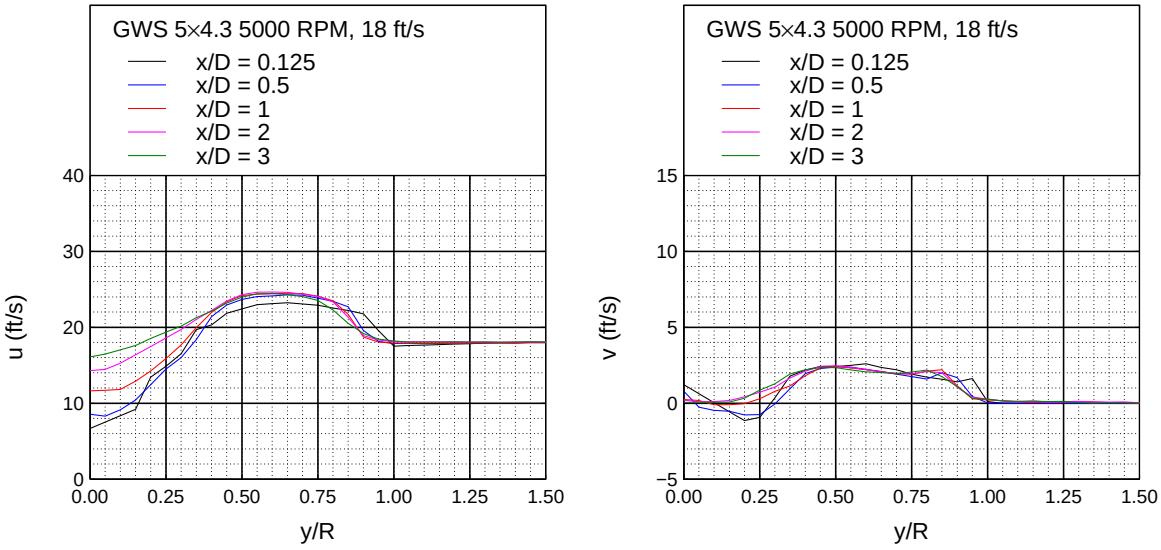

(a) (b)

Figure 22: Velocity measurements from the slipstream of the GWS 5×4.3 at 5,000 RPM and 18 ft/s ($J = 0.52$): (a) axial velocity and (b) swirl velocity.

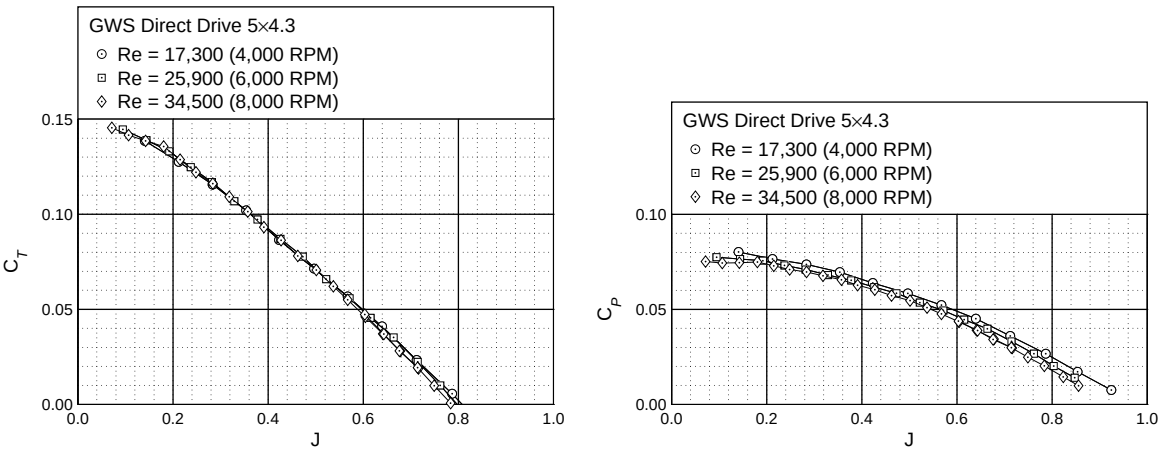

(a) (b)

Figure 23: GWS Direct Drive 5×4.3 advancing-flow performance: (a) thrust coefficient and (b) power coefficient.

thrust due to the difficultly in measuring the outer edge of the slipstream; the outer velocities were either too small or at too large of an angle for the 7-hole probe to measure. Table 1 shows the thrust calculated from the advancing-flow slipstreams for a few propellers. The thrust measurements are from the advancing-flow performance tests found in Deters et al.[4,5] and on the UIUC Propeller Database.[20] Results from the slipstream measurements are a reasonable estimate to the measured thrusts with differences around 15% and less.

Ideally the thrust should be measured from the difference in the static pressure behind the propeller and ahead of it. The 7-hole probe provides the static pressure difference, but the static pressure ahead of the propeller is not known. An estimate of the static pressure ahead of the propeller can be made by assuming the axial velocity measured at the closest position downstream of the propeller is the same as the velocity just ahead of the propeller. Momentum theory states that the velocity through the propeller is continuous while there is a discontinuous pressure increase. This assumption also ignores any frictional losses imparted

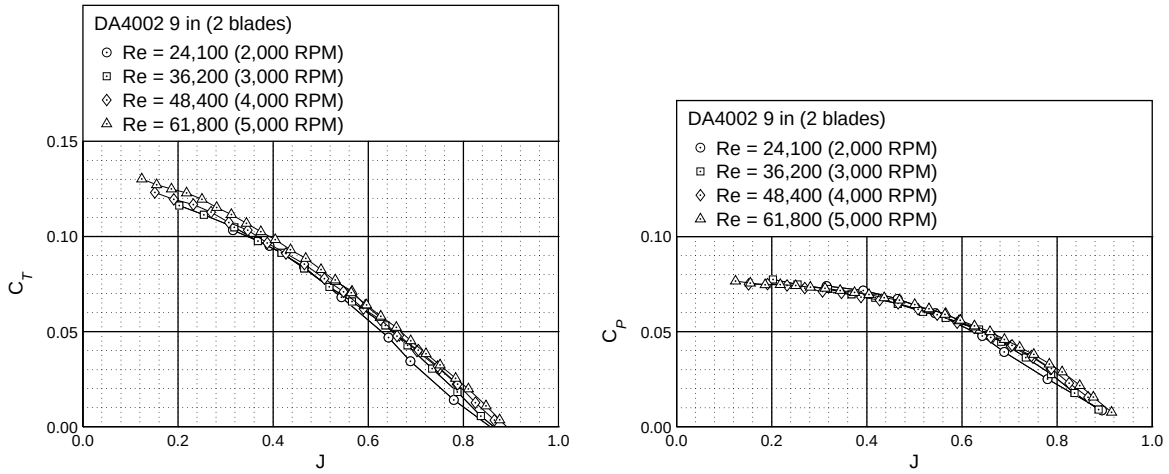

(a) (b)

Figure 24: DA4002 9×6.75 advancing-flow performance: (a) thrust coefficient and (b) power coefficient.

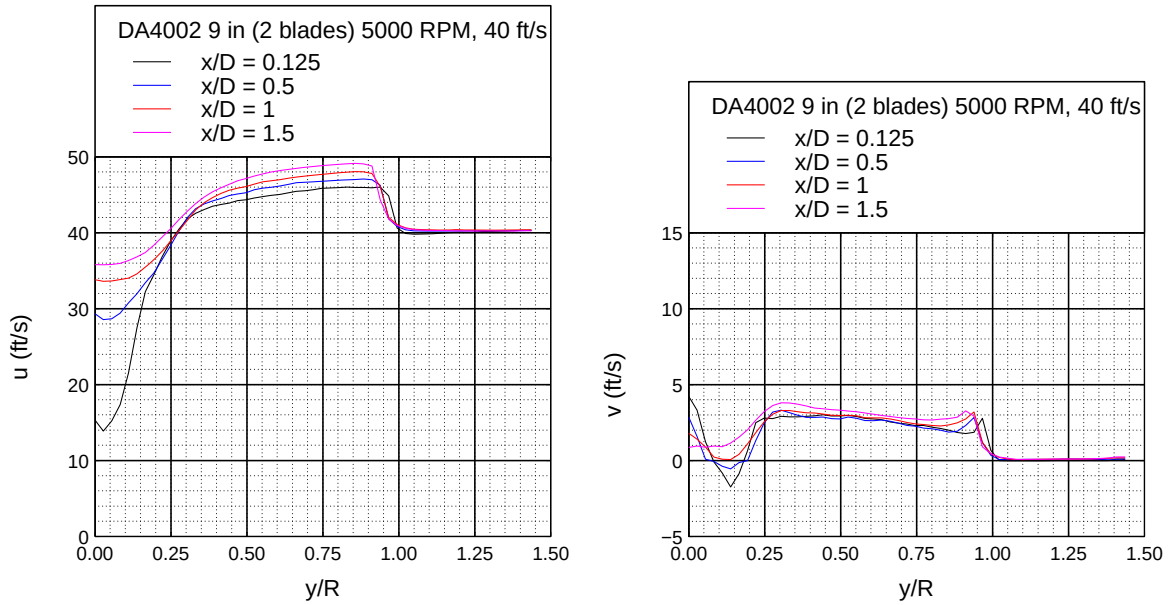

(a) (b)

Figure 25: Velocity measurements from the slipstream of the DA4002 9 in propeller at 5,000 RPM and 40 ft/s ($J = 0.64$): (a) axial velocity and (b) swirl velocity.

by the propeller blades. Momentum thoery also assumes that the velocity is uniform along the propeller, but slipstream measurements clearly show that this is not the case. From Bernoulli's equation, the static pressure ahead of the propeller can be found from the total pressure and the velocity at the propeller by

$$p_1 = p_{0_u} - \frac{1}{2}\rho V_1^2 \tag{24}$$

The total pressure was assumed to be uniform ahead of the propeller based on experiments done by Stanton et al.[6] and Fage et al.[7] Using the axial velocity behind the propeller for the velocity V_1, the static pressure ahead of the propeller was estimated. Since the measured axial velocities were not constant along the propeller, the calculated pressures ahead of the propeller were not constant. Using the static pressures calculated from Eq. 24 and the static pressures found from the 7-hole probe, the thrust was calculated.

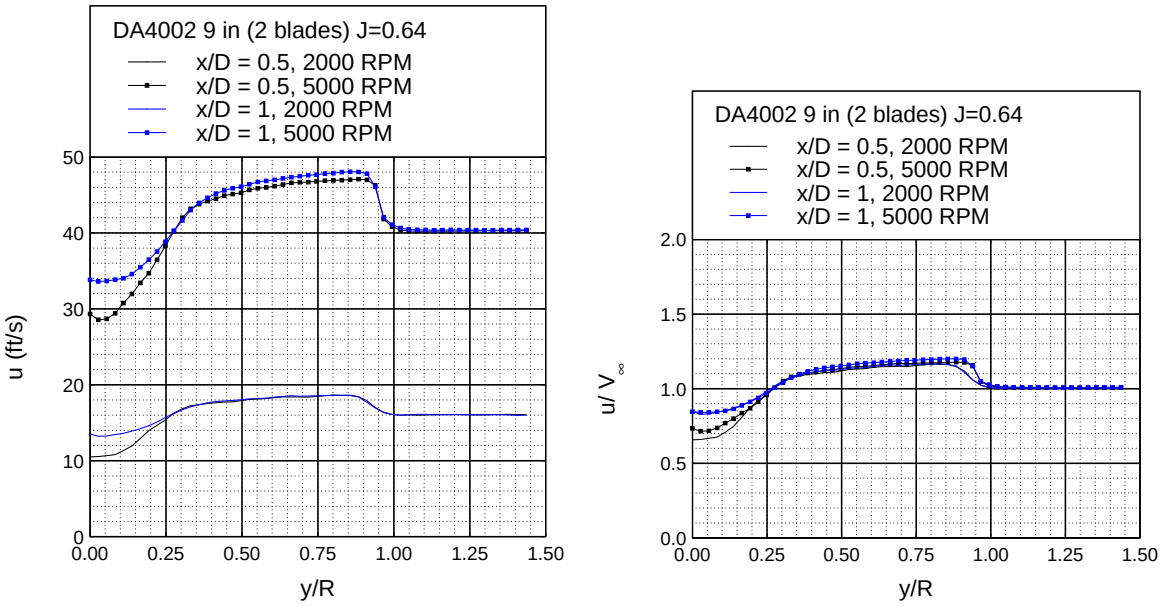

Figure 26: Velocity comparison for the DA4002 9 in propeller at the same advance ratio ($J = 0.64$) but at different rotation rates: (a) axial velocity and (b) u/V_∞.

Table 1: Load Cell and Slipstream Thrust Measurements

Propeller	RPM	Velocity	Force measurements (oz)	Slipstream method (oz)	Difference
5 in DA4002	6,000	26	0.62	0.66	5.97%
2 blade	7,500	34	1.01	0.89	12.0%
9 in DA4002	2,000	16	0.59	0.52	12.6%
2 blade	5,000	36	5.84	5.11	12.6%
9 in DA4022	2,000	10	1.31	1.11	15.3%
2 blade	2,000	14	0.87	0.74	15.2%
5 in NR640	6,000	20	0.38	0.38	2.19%
2 blade	10,000	34	1.36	1.22	10.5%
9 in NR640	3,000	18	0.83	5.79	7.20%
2 blade	6,000	36	4.98	4.52	9.39%

Table 2 shows the thrust calculated using the slipstream total pressure difference and the slipstream static pressure difference for the DA4002 propellers. It seems that the static pressure method estimates a lower thrust, and in general using the total pressure provides a better estimate. By using a pitot probe that is fairly insensitive to the flow angle, the thrust of a propeller can be estimated by the total pressure measurements behind the propeller. Total pressure measurements should be taken as close to the propeller as possible for the best results as shown in Table 3 for the 5 in NR640 at 6,000 RPM and 20 ft/s. Further downstream, the thrust calculated from the total pressure difference becomes smaller.

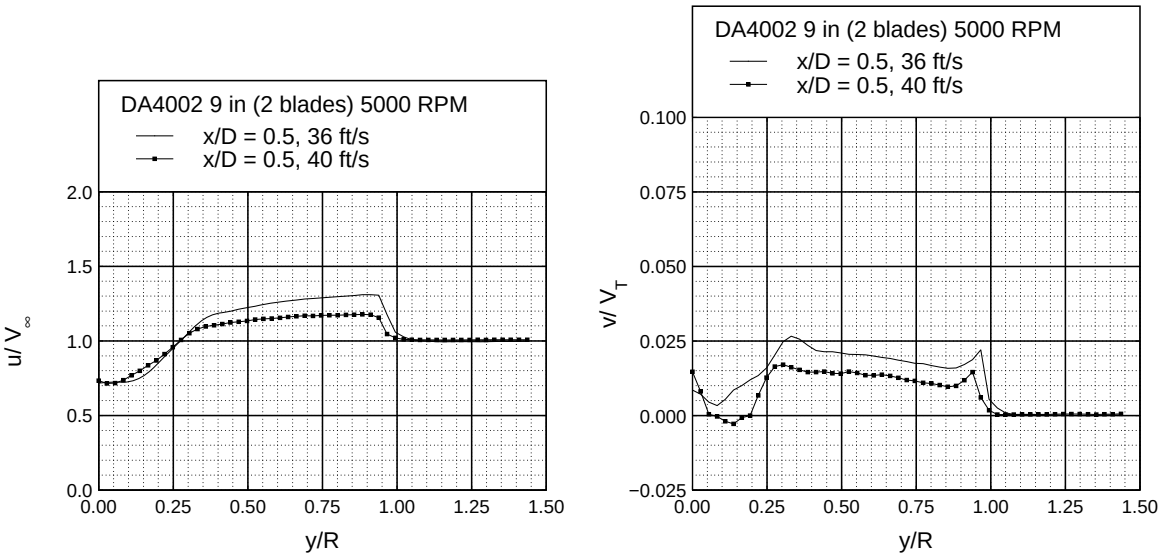

(a) (b)

Figure 27: Velocity comparison for the DA4002 9 in propeller at 5,000 RPM at different advance ratios: (a) u/V_∞ and (b) v/V_T.

Table 2: Slipstream Thrust Measurements from Total and Static Pressures

Propeller	RPM	Velocity	Thrust (oz) [Total Pressure]	Thrust (oz) [Static Pressure]
5 in DA4002	6,000	26	0.66	0.61
2 blade	7,500	34	0.89	0.77
9 in DA4002	2,000	16	0.52	0.49
2 blade	5,000	36	5.11	4.64

Table 3: Slipstream Thrust Measurements for the 5 in NR640 at 6,000 RPM and 20 ft/s

x/D	Thrust (oz)
0.125	0.38
0.500	0.33
1.000	0.33
2.000	0.30
3.000	0.30

C. Wing Effect on Static Slipstream

In the previous sections, the slipstreams discussed were for an isolated propeller. These slipstreams are very useful for describing the flow from a small rotorcraft such as a quadrotor or the flow directly behind a propeller before it interacts with a lifting surface of an aircraft such as a wing. When a propeller slipstream encounters a surface like a wing, the rotational part of the slipstream will be impeded by the wing, and skin friction from the wing will also affect the motion of the propeller slipstream. The resulting propeller-wing flow will be different than the flow behind just a propeller.

To study the effect of a wing on the propeller slipstream, a flat-plate wing was placed behind a propeller and tested during static conditions, which would represent a small aircraft in hover. Many small aircraft have a large enough thrust-to-weight ratio that allows the aircraft to hover using only the thrust of the propeller to counter the weight of the aircraft. During hover, the aircraft is oriented vertically and looks to be "hanging" by the propeller, which is why this maneuver is sometimes called prop hanging. The control surfaces of the wing and tail are used to control the aircraft, and they must rely on the flow from the propeller slipstream in order to generate any aerodynamic forces. Due to the wing-propeller interaction, the propeller slipstream seen by the tail will be different than the slipstream seen by the wing.[23,24]

The results of one propeller tested with the flat-plate wing are presented in this section; results from two additional propellers can be found in Deters.[4] The 5 in DA4002 with two blades was tested with the leading edge of the wing at 0.5D (2.5 in) and at 0.125D (0.625 in) downstream. For the wing-propeller slipstream measurements, the wing was horizontal and set to an incidence angle of 0 deg with the leading edge aligned with the center of the propeller. For the case where the wing was located 0.5D downstream, slipstream measurements were taken at 1.5 and 2D (7.5 and 10 in) behind the propeller. With respect to the wing, the measurements were taken 1.5 and 4 in behind the trailing edge. For the case where the wing was located 0.125D downstream, the slipstream was measured at 1, 1.5, and 2D (5, 7.5, and 10 in) behind the propeller or 4.125, 6.625, and 9.125 in from the trailing edge of the wing. Since the wing-propeller slipstream was no longer axisymmetric, vertical slices at multiple wingspan locations were taken in order to have a more complete picture of the slipstream.

Slipstream measurements for the propeller-only case of the DA4002 are shown in Fig. 28. The vectors show the swirl velocity, and the contour shows the axial velocity in ft/s. The distances along the axes are nondimensionalized by the propeller radius of 2.5 in with x along the span of the wing and y above (positive) or below (negative). From the direction of the swirl vectors, the plot is a view of the plane looking towards the propeller from downstream. As seen in the figure, the propeller slipstream is basically axisymmetric. As was shown in the static slipstream results (Section IV-A), the propeller slipstream expands, and both the axial and swirl velocities decrease.

Figure 29 shows the results for the case with the wing 0.125D behind the propeller. The wing-propeller slipstream is clearly not axisymmetric, and the wing looks like it has caused the upper and lower parts of the slipstream to separate and diverge. As the slipstream moves downstream, the location of maximum axial and swirl velocities on the upper and lower parts of the slipstream move farther apart in the direction of their respective swirl velocities. Results for the wing 0.5D behind the propeller are shown in Fig. 30. Similar to the wing at 0.125D, the wing at 0.5D causes the slipstream to split and the upper and lower portions to diverge. However, the amount of movement away from the center is less than the 0.125-D case.

While the wing causes the maximum axial and swirl velocities to move away from the center of the propeller, it can be seen in Figs. 28–30 that the maximum velocities at each downstream location still have about the same magnitude. Figure 31 shows the velocities measured 2D downstream at the wingspan locations where the axial and swirl velocities were the greatest. For the propeller-only case, the velocities are at the propeller center (0 in); for the wing at 0.125D, the velocities were measured 2 in ($x/R = 0.8$) from the center, and for the wing at 0.5D, the velocities were measured 1 in ($x/R = 0.4$) from the center. As seen in the figure, the axial velocities for all three cases are very similar. For the swirl velocities, the three cases are very close past $y/R = 0.5$.

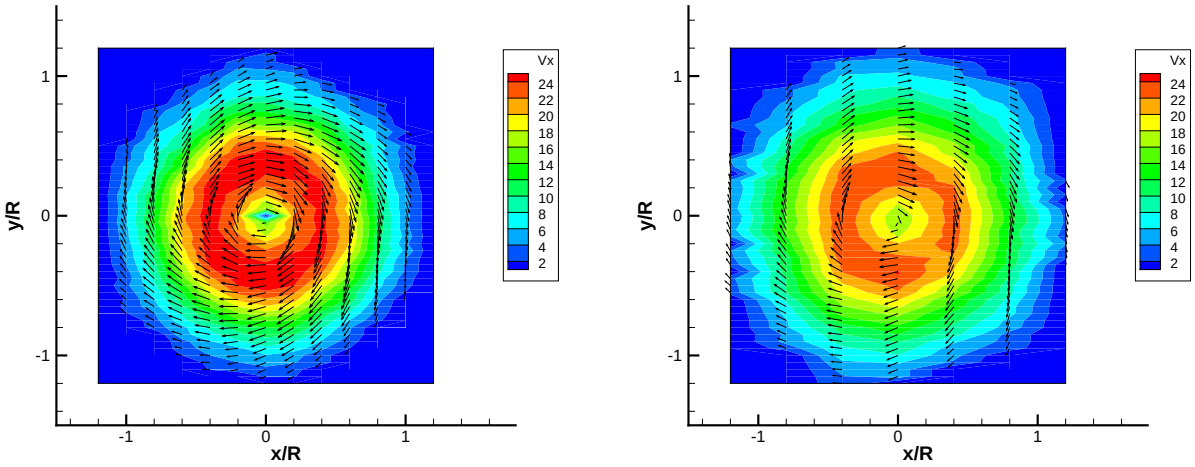

(a) $x/D = 1$

(b) $x/D = 1.5$

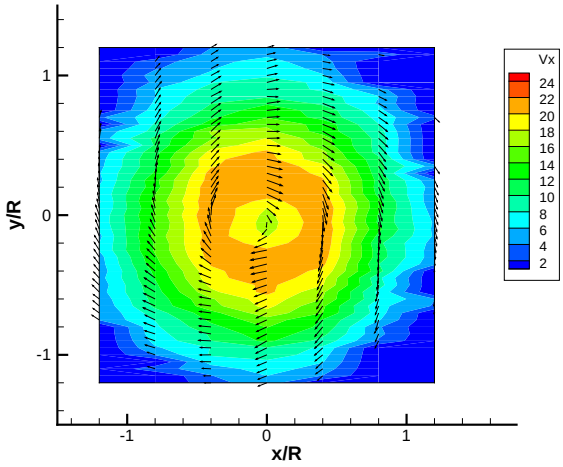

(c) $x/D = 2$

Figure 28: Slipstream measurements of the 5 in DA4002 propeller. Velocities are in ft/s.

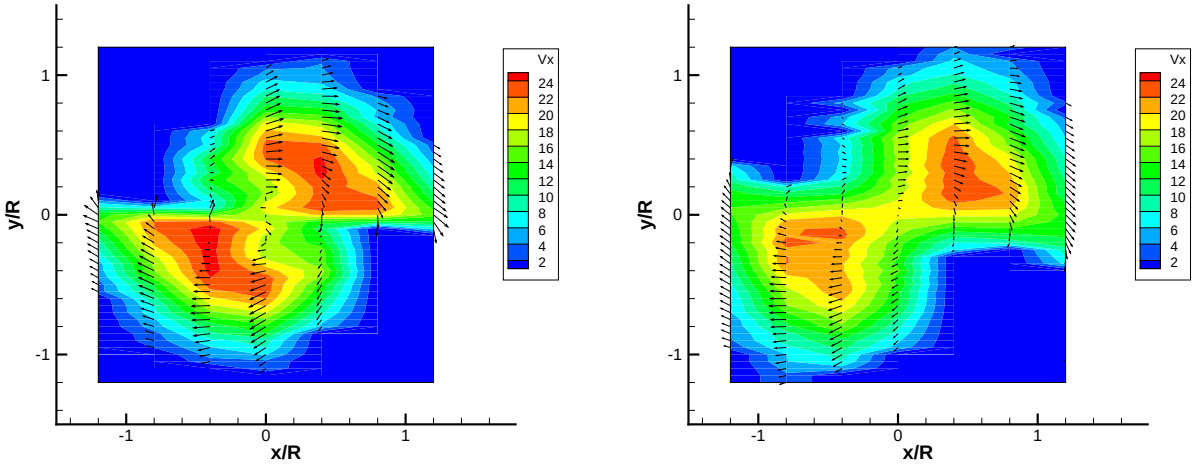

(a) $x/D = 1$

(b) $x/D = 1.5$

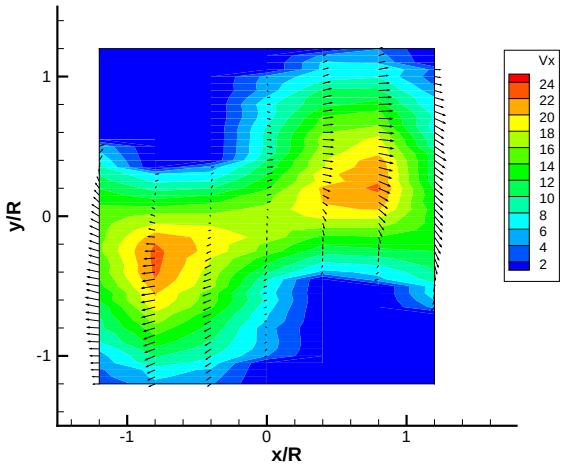

(c) $x/D = 2$

Figure 29: Slipstream measurements of the 5 in DA4002 propeller with the flat-plate wing at 0.125D behind the propeller. Velocities are in ft/s.

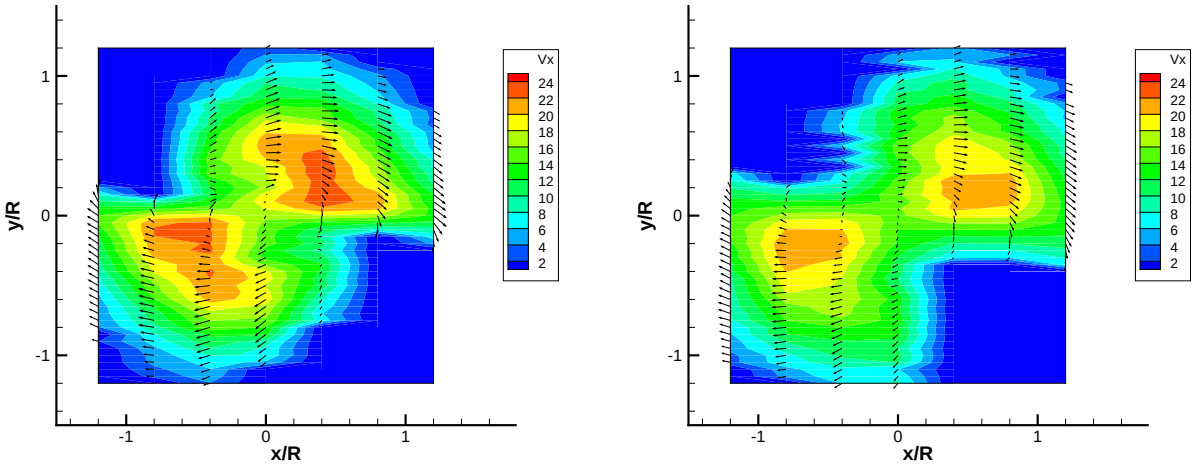

(a) $x/D = 1.5$ (b) $x/D = 2$

Figure 30: Slipstream measurements of the 5 in DA4002 propeller with the flat-plate wing at 0.5D behind the propeller. Velocities are in ft/s.

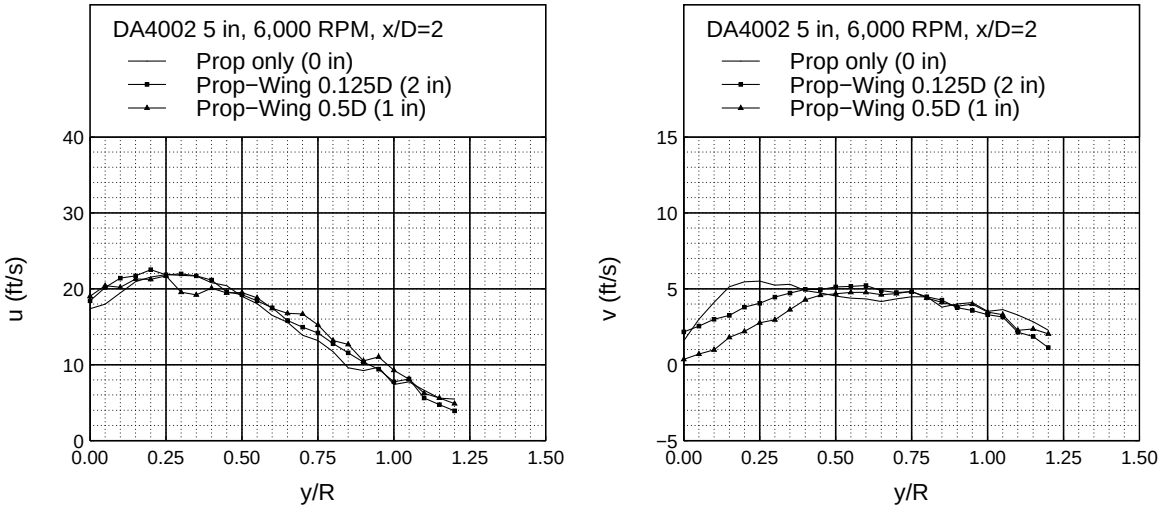

(a) (b)

Figure 31: Slipstream measurements at $x/D = 2$ of the DA4002 5-in propeller at 6,000 RPM with a flat-plate wing. Propeller-wing measurements are offset in the span direction of the wing: (a) axial velocity and (b) swirl velocity.

V. Conclusions

Slipstream measurements were successfully measured using a 7-hole probe. For the static conditions, the slipstream expands with both the magnitudes of the axial and swirl velocity profiles decreasing as the slipstream moves downstream. While a variety of propellers with different planform shapes were tested, the general shape of the axial velocity profile was the same. The maximum axial velocity would occur near the 75% blade station close to the propeller and moved towards the center as the slipstream progressed downstream. From the APC static condition results, it was shown that if Reynolds number effects were seen in the static thrust coefficient, then Reynolds number effects were also seen in the axial velocity ratio. In other words, as the thrust coefficient increased, the axial velocity ratio increased. However, the amount of change in the axial velocity ratio was small and less than what was predicted by momentum theory. The static slipstream results presented in this paper showed that if the slipstream velocities were known for a propeller at one rotational rate, the velocities at another rotational rate could be estimated by scaling the velocities by the tip speed and accounting for any Reynolds number effects.

During advancing-flow conditions, the slipstream was seen to contract instead of expand. The minimum size of the slipstream was seen to occur by $x/D = 0.5$. Unlike the static slipstreams, the shape of the axial velocity profile for each propeller was dependent on the planform of the propeller. Reynolds number effects on the thrust coefficient could be seen in the advancing flow slipstreams as an increase in the ratio of the axial velocity to the freestream velocity. Using the total pressure measurements from the advancing-flow slipstreams, an estimate of the thrust of the propeller could be made.

Finally the effect of a flat-plate wing on a propeller slipstream was measured during static conditions. When a flat plate splits the slipstream, both halves move away from each other in the direction of their respective swirl velocities. While the wing separates the upper and lower parts of the slipstream, it does not in fact lower the axial or swirl velocities. How far the halves of the slipstream move away from each other is dependent on how close the wing is to the propeller. At two diameters downstream, the location of the maximum axial and swirl velocities were 2 in from the propeller centerline for the 0.125D wing case and were located 1 in from the centerline for 0.5D wing case.

Acknowledgments

The authors would like to thank Matthew Dempsey and Rushant Badani for their help in taking propeller slipstream wind tunnel data.

References

[1]Johnson, W., *Helicopter Theory*, Dover Publications, Inc., New York, 1980.

[2]Leishman, J. G., *Principles of Helicopter Aerodynamics*, Cambridge University Press, Cambridge, 2000.

[3]McCormick, B. W., *Aerodynamics, Aeronautics, and Flight Mechanics*, John Wiley and Sons, Inc, New York, 1995.

[4]Deters, R. W., "Performance and Slipstream Characteristics of Small-Scale Propellers at Low Reynolds Numbers," Ph.D. Dissertation, Department of Aerospace Engineering, University of Illinois at Urbana-Champaign, Urbana, IL, 2014.

[5]Deters, R. W., Ananda, G. K., and Selig, M. S., "Reynolds Number Effects on the Performance of Small-Scale Propellers," AIAA Paper 2014-2151, 2014.

[6]Stanton, T. E. and Marshall, D., "On a Method of Estimating, from Observations of the Slipstream of an Airscrew, the Performance of the Elements of the Blades, and the Total Thrust of the Screw," Aeronautical Research Committee R&M 460, 1918.

[7]Fage, A. and Howard, R. G., "An Experimental Investigation of the Nature of the Airflow around an Airscrew in order to Determine the Extent to which the Airflow Assumed in the Momentum Theory of Froude is Realised in Practice," Aeronautical Research Committee R&M 565, 1919.

[8]Fage, A., "A Note on the Method of Estimating from Observations of Total Head, the Total Thrust of an Airscrew," Aeronautical Research Committee R&M 699, 1920.

[9]Fage, A. and Howard, R. G., "A Consideration of Airscrew Theory in the Light of Data Derived from an Experimental Investigation of the Distribution of Pressure over the Entire Surface of an Airscrew Blade and Also over Aerofoils of Appropriate Shapes." Aeronautical Research Committee R&M 681, 1921.

[10]Khodadoust, A., "An Experimental Study of the Flowfield on a Semispan Rectangular Wing with a Simulated Glaze Ice Accretion," Ph.D. Dissertation, Department of Aeronautical and Astronautical Engineering, University of Illinois at Urbana-Champaign, Urbana, IL, 1993.

[11]Aeroprobe website, http://www.aeroprobe.com, Accessed May 27, 2015.

[12]Ananda, G. K., Deters, R. W., and Selig, M. S., "Propeller-Induced Flow Effects on Wings of Varying Aspect Ratio at Low Reynolds Numbers," AIAA Paper 2014-2152, 2014.

[13]Ananda, G. K., Sukumar, P. P., and Selig, M. S., "Measured Aerodynamic Characteristics of Wings at Low Reynolds Numbers," *Aerospace Science and Technology*, Vol. 42, 2015, pp. 392–406.

[14]Gallington, R. W., "Measurement of Very Large Flow Angles with Non-Nulling Seven-Hole Probes," USAFA-TR-80-17, 1980.

[15]Gerner, A. A., Maurer, C. L., and Gallington, R. W., "Non-Nulling Seven-Hole Probes for High Angle Flow Measurement," *Experiments in Fluids*, Vol. 2, 1984, pp. 95–103.

[16]Zilliac, G. G., "Calibration of Seven-Hole Pressure Probes for Use in Fluid Flows with Large Angularity," NASA TM 102200, 1989.

[17]Zilliac, G. G., "Modelling, Calibration, and Error Analysis of Seven-Hole Pressure Probes," *Experiments in Fluids*, Vol. 14, 1989, pp. 104–120.

[18]Barker, M., "On the Use of Very Small Pitot-Tubes for Measuring Wind Velocity," *Proceeding of the Royal Society A*, Vol. 101, 1922, pp. 435–445.

[19]Bryer, D. W. and Pankhurst, R. C., *Pressure-Probe Methods for Determining Wind Speed and Flow Direction*, Her Majesty's Stationery Office, London, 1971.

[20]Selig, M. S., UIUC Applied Aerodynamics Group, http://aerospace.illinois.edu/m-selig/, Accessed May 27, 2015.

[21]Khan, W. and Nahon, M., "Development and Validation of a Propeller Slipstream Model for Unmanned Aerial Vehicles," *Journal of Aircraft*, DOI: 10.2514/1.C033118.

[22]Pannell, J. R. and Jones, R., "An Investigation into the Nature of the Flow in the Neighbourhood of an Airscrew," Aeronautical Research Committee R&M 371, 1917.

[23]Selig, M. S., "Modeling Propeller Aerodynamics and Slipstream Effects on Small UAVs in Realtime," AIAA Paper 2010-7936, 2010.

[24]Selig, M. S., "Real-Time Flight Simulation of Highly Maneuverable Unmanned Aerial Vehicles," *Journal of Aircraft*, Vol. 51, No. 6, November–December 2014, pp. 1705–1725.